

Article

# Characterizations of Efficient Charge Transfer and Photoelectric Performance in the Cosensitization of Solar Cells

Qian Liu <sup>1,2</sup>, Xiaochen Lin <sup>3</sup>, Lu Mi <sup>2</sup>, Nan Gao <sup>2</sup>, Peng Song <sup>4,\*</sup> , Fengcai Ma <sup>4</sup> and Yuanzuo Li <sup>2,\*</sup><sup>1</sup> Department of Applied Physics, Xi'an University of Technology, Xi'an 710054, China; liuqian@xaut.edu.cn<sup>2</sup> College of Science, Northeast Forestry University, Harbin 150040, China; milufine@sina.com (L.M.); nan\_g@nefu.edu.cn (N.G.)<sup>3</sup> Chemical Industry and Material College, Heilongjiang University, Harbin 150080, China; xiaochenlinhd@sohu.com<sup>4</sup> Department of Physics, Liaoning University, Shenyang 110036, China; mafengcai@lnu.edu.cn

\* Correspondence: songpeng@lnu.edu.cn (P.S.); yzli@nefu.edu.cn (Y.L.); Tel.: +86-24-6220-2365 (P.S.); +86-451-8219-2245 (Y.L.)

Received: 2 June 2018; Accepted: 4 July 2018; Published: 11 July 2018



**Abstract:** Dyes D35 and XY1 for solar cells have been investigated theoretically with the quantum chemistry method and visualized 3D cube representation. Some important information (such as absorption spectra, molecular orbitals, reorganization energy, chemical reactivity, driving force of electron injection, light-harvesting efficiency, as well as the dipole moment, etc.) has been studied to explain the efficiency of dyes, and the visualized intramolecular and intermolecular charge transfer process and fast dynamic process of the interface electron transfer have been studied to estimate the strength of electron transfer in cosensitization. Calculated results indicated that the improved absorption spectra range, fast electron injection, and the larger dipole moment significantly promote the cosensitized solar cell efficiency in comparison with isolated Dye-Sensitized Solar Cells (DSSCs).

**Keywords:** DSSCs; charge transfer; cosensitized solar cell; density functional theory

## 1. Introduction

Organic solar cells have become one of the substitutes for traditional silicon solar cells owing to its merits (clean, environmentally friendly, no pollution, etc.) [1]. As an important photodevice, Dye-Sensitized Solar Cells (DSSCs) display many advantages and have been paid considerable attention [2,3], and their working processes can be briefly described as below [4]. During absorption of sunlight, sensitive dye is excited, forming an excited state, and electrons are subsequently shifted into TiO<sub>2</sub>. This process is designated as the electron injection process. Subsequently, electrons reach the external circuit and generate an electric current. Dyes with a loss of electrons can be recovered from electrolytes. In these working cycles, one important process is the efficiency of strong molecular absorption and efficient charge separation [4].

The electronic transition with strong absorption results in more electrons and hole accumulation in TiO<sub>2</sub> nanoparticles and dyes, respectively, which corresponds to a Charge Transfer (CT) state. This means that a CT excited state with strong absorption is a photoinduced CT complex [5]. A weak absorption was also found in intermolecular CT for donor–acceptor dyad, and intramolecular CT leads to strong absorption in the dye with a donor– $\pi$ –acceptor structure. After photoexcitation, the excitons on the molecule are usually dissociated to electron–hole pairs, intramolecular CT occurs, and the electrons are shifted from molecule to TiO<sub>2</sub> nanoparticles. Apart from CT, a matching of absorption spectra is hoped for full utility of sunlight. Because it is difficult for a single dye to cover the

ultraviolet and near-infrared region, cosensitization provides a way with a variety of complementary dyes in order to broaden the absorption spectra range and strength [6–11]. A series of porphyrin dyes (XW1–XW4) cosensitized with Dye C1, in which highest cell efficiency has reached 10.45% [11], and the absorption band from dye C1 makes up for poor absorption in 500 nm for porphyrin dye. Zhu et al. used the coabsorption/cosensitization based on a phenothiazine-based electron donor to improve conversion for nonruthenium solar cells (reported to be 11.5%) [6]. PTZ-2 and N719 in phenothiazine-based cosensitization possess efficiency of 8.12% compared with PTZ-2 (5.81%) and N719 (6.97%) [7]. The cosensitization (D35 and XY1) displays a higher VOC and improves conversion efficiency [12]. As an auxiliary means for experiment, quantum chemistry methods were universally used to deal with the structure, spectra, and excited state properties of multibranch dyes [13,14], metal-free dyes with multidonor moiety [15], natural dyes [16,17], and metal-containing dyes [18–20].

In this work, we performed a quantum chemistry calculation to research the geometries, spectra, CT processes, and photoelectric properties for the DS-35, XY1, and cosensitization systems. Important characteristics for intramolecular CT in a single dye attached to TiO<sub>2</sub> were estimated, which were compared with intermolecular CT for cosensitization systems between DS-35 and XY1, owing to the fact that there is competition for CT and charge loss. Furthermore, photoelectric properties of single dyes and cosensitization systems were studied to reveal the different performance in solar cells. The current investigation provides a clue for understanding the micromechanism and deduces the possible reason why a cosensitization system has good efficiency in the field of solar cells.

## 2. Calculated Methods

Current work was calculated with the Gaussian software 09 [21]. For D35 and XY1 geometric optimizations (see Figure 1), we used density functional theory (DFT) [22], B3LYP [23–25], and 6–31 (d) basis set. Absorption spectra and fluorescence were done with time-dependent DFT (TD-DFT) theory [26] using the Cam-b3lyp functional [27], 6–31 (d) basis set. The solvent effect (solvent = acetonitrile) with the CPCM model was included in calculation [28]. The ground state geometry of dyes attached to TiO<sub>2</sub> clusters was optimized with the same functional, and 6–31 (d) basis set for N, S, C, H, O, and LANL2DZ functional [29] for Ti. Electronic transitions of Dye/TiO<sub>2</sub> were calculated with TD-DFT//Cam-B3LYP and the same setup of basis set as the optimization. The dimer of D35 and XY1 was optimized with the DFT//B3LYP/6–31 (d), the absorption spectra were calculated with TD-DFT//Cam-B3LYP/6-31 (d), and the intermolecular CT was estimated from Marcus theory [30]. The electron injection from dye to semiconductor was calculated with the Newns–Anderson model [31,32]. A 3D cube representation of photon-induced charge using different density was performed to investigate the electronic density change in the smaller molecular solar cell [33].

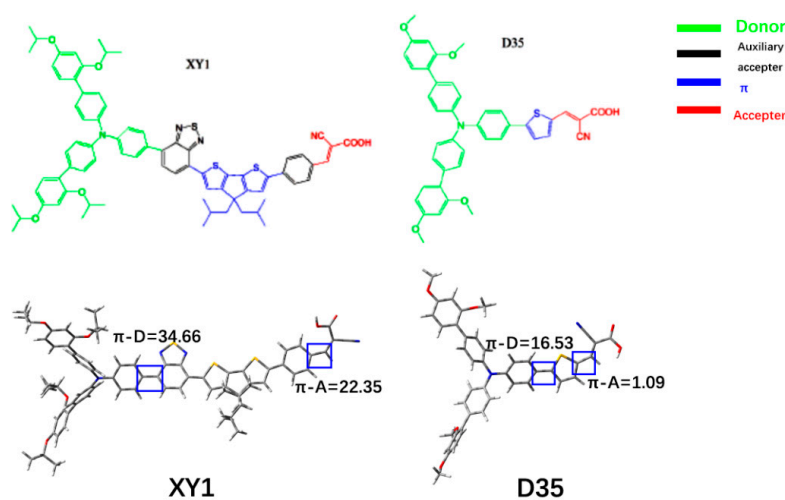


**Figure 1.** Chemical and optimized structures for D35 and XY1, respectively.

### 3. Results and Discussion

#### 3.1. Structure

Figure 1 shows the optimized molecular structures of dyes XY1 and D35; here, dye XY1 containing the bulky donor, CPDT (cyclopentadithiophene) conjugated bridge introduced with a benzene ring, accessory receptor BTZ, and the expanded range of donor and acceptor can cause higher absorption spectra characteristics. For the arylamine-based dye D35, it possesses a donor–bridge–acceptor structure that is different from the XY1 structure, and the higher (open-circuit photovoltage) VOC has been obtained with the inhibition of electron reception from TiO<sub>2</sub>. The structure of donor–bridge–acceptor is a usual structure and has been proven to be beneficial to enhancing electron injection and recovery of excited dye. It is hoped that the spectra and energy levels can be satisfactory, matching the coupling of the two kinds of dyes in designing solar cells.

As shown in Figure 1, the two isolated dyes in acetonitrile solvent display special dihedral angles of 1.09° and 22.35° degree for D35 and XY1 between the thiophene and benzene and hydroxy acrylic acid. Compared with the XY1, D35 tends for the coplanar structure, and electrons are easily moved from donor to acceptor through the conjugated bridge, and further injected into TiO<sub>2</sub>. At the same time, D35 exhibits a well-conjugated degree in the middle region of molecular structure (i.e., dihedral angles are 16.53 for D35 and 34.66 for XY1, respectively). It is worth noting that the twisted angles among donor units for XY1 are larger than those of D35 that can reduce the dyes' aggregation due to the repellent interaction.

#### 3.2. Energy Levels

Figure 2 shows the Highest Occupied Molecular Orbital (HOMO) and Lowest Unoccupied Molecular Orbital (LUMO) levels for two dyes, and Table S1 lists the energy data and energy gap. From Figure 2, it was found that the energy level of the TiO<sub>2</sub> semiconductor (4.0 eV) is much less than the energy level of the LUMO dyes, which is beneficial to the electronic injection (excited dye → TiO<sub>2</sub>). Comparing the LUMO of the two dyes, it was found that D35 is higher than that of XY1, meaning that CT could take place from LUMO of D35 to XY1, producing intermolecular CT. Furthermore, the higher HOMO energy level for XY1 can minimize energy gap (D35 and XY are 2.28 and 1.98 eV, respectively), leading to the red-shifted absorption peak. The smaller band of cosensitized system should reflect the tendency of broadened absorption spectra, which will compensate for the inadequacies of isolated dye absorption. The improvement in spectra for cosensitization will enhance the solar utilization affecting the overall efficiency. For cosensitized systems (D35 + XY1), the energy gap is close to that of the XY1 due to the near HOMO energy level with XY1 that can be chalked up to the contribution of XY1 for cosensitized HOMO (see Table S1). As a whole, energy levels of XY1, D35, and XY1 and D35 have good matching with the semiconductor band.

Upon dye adsorption on TiO<sub>2</sub>, the energy level will be changed, as shown in Figure 2. Adsorption energy ( $E_{ads}$ ) was calculated by the strong interaction energy of dye–TiO<sub>2</sub> ( $E_{dye+TiO_2}$ ) and the isolated dye ( $E_{dye}$ ) and TiO<sub>2</sub> ( $E_{TiO_2}$ ); that is to say,  $E_{ads} = E_{dye+TiO_2} - (E_{dye} + E_{TiO_2})$ , and XY1 (−4.04) < D35 (−4.03), which are almost the same negative values, displaying the stable configuration. The HOMO level of D35 and D35–TiO<sub>2</sub> is −5.03 eV and −4.97 eV, respectively, with very little change. LUMO (−2.81 eV) for D35–TiO<sub>2</sub> is lower than that of isolated dye D35 (−2.75). Similar trends were found in XY1 and XY1–TiO<sub>2</sub>. Given that HOMO levels are closely related to donors and LUMO levels mainly affected by receptors, dye adsorption in semiconductor will result in strong electron coupling and cause the lower LUMO. In addition, energy gap is decreased compared to the isolated dye; however, the decreased value of energy gap is at the same level.

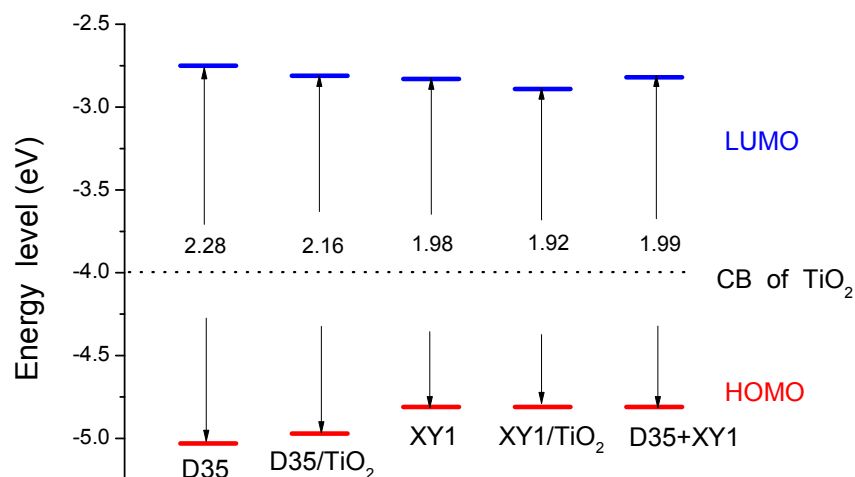


**Figure 2.** Energy levels of the isolated dye in acetonitrile and its adsorption spectrum on  $\text{TiO}_2$  as well as cosensitized molecular system.

### 3.3. Absorption Spectra

Based on the optimized molecular structures, we used the TD-DFT method to study the absorption spectra for dyes D35, D35- $\text{TiO}_2$ , XY1, XY1- $\text{TiO}_2$ , and cosensitized molecular system. Figure 3 shows that Dye D35 has a wide absorption range in the visible region with two prominent peaks, in which the strongest absorption peak is found in 453 nm that also contributed to HOMO-LUMO transition (see Table S2), and this state has a larger oscillator strength ( $f = 1.36$ ). Because the HOMO electron cloud is concentrated on the whole molecular skeleton and LUMO resides in the bridge and acceptor units (see electron density distribution in Figure S1), the first excited state will result in efficient intramolecular CT.

Figure 4 shows the Charge Different Density (CDD) for calculated excited states. For the S1 state, red electron is moved in a direction of the acceptor; the green hole resides in the donor unit, resulting in the electron transfer from donor to acceptor. For another excited state (S2) of D35, electron transition is composed of HOMO  $\rightarrow$  LUMO + 2, having a weight of 74%, which state is also an intramolecular CT from the triarylamine unit to cyanoacrylic acid. The above states exhibit a strong push-pull behavior characteristic. States S4 and S5 are also ICT states with the same characteristics as S1. Located excited state is found to be the S3 state that is an excitation of donor and bridge.

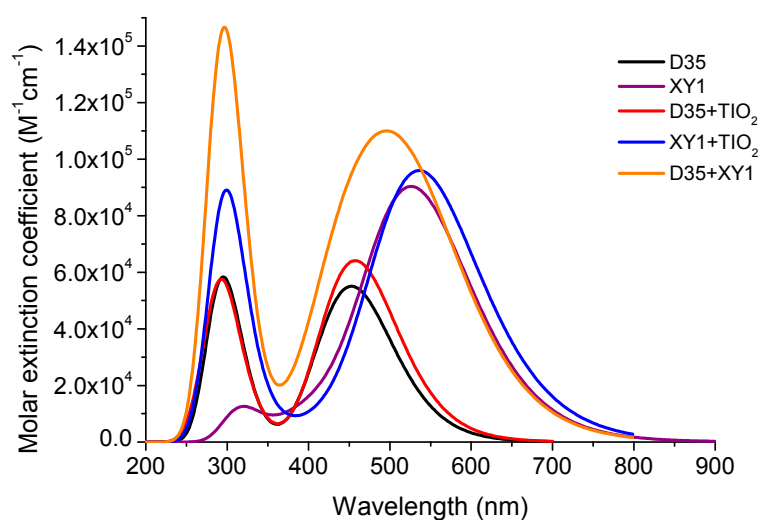


**Figure 3.** Simulated spectra for the dye in acetonitrile solvent, adsorption on  $\text{TiO}_2$  and cosensitization.

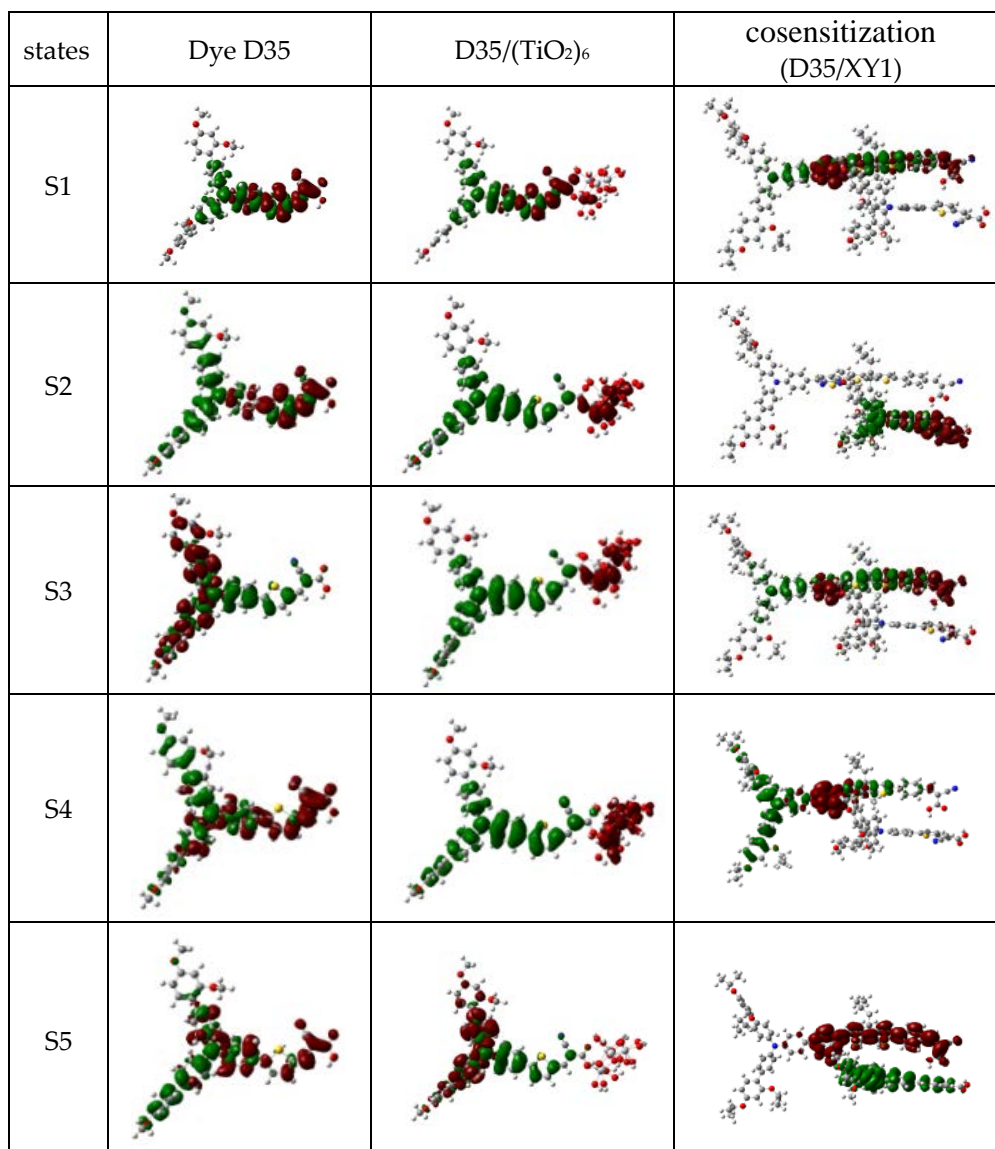


**Figure 4.** Intramolecular and intermolecular CT (charge transfer) for the dye/TiO<sub>2</sub> and the cosensitized systems.

XY1 has a wide range of spectral response and strong absorption intensity at 529 nm, which come mainly from electronic transition (HOMO → LUMO). Stronger absorption can make up for the deficiency of D35 in the range above 500. From absorption spectra in Figure 3, red-shifted movement for the first peak for dye–TiO<sub>2</sub> occurs compared with the isolated molecules, which can be attributed to the change of energy gap; moreover, the molar extinction coefficient has been improved to enhance the photoabsorption efficiency. For cosensitized molecular systems, XY1 and D35 have two absorption bands, and the first absorption is found at 530 that are close to the value of XY1 (see Table S2). There exists an influence of local electric field caused by the solar cell electrode, and some characteristics (such as absorption, dipole moment, and polarizability) should be changed by the local electric field (three fields  $(10, 20, 30) \times 10^{-4}$  a.u.). Under an electric field condition of  $10 \times 10^{-4}$  a.u., absorption peak of XY1 and D35 has changed about 6 nm compared with the nonelectric field (see Table S3), and oscillator is reduced about 0.2; As the electric fields ( $20 \times 10^{-4}$  a.u. and  $30 \times 10^{-4}$  a.u.) increase, the absorption spectra make obviously red-shifted, i.e., the maximum absorption wavelength is

563.65 nm ( $f = 1.5047$ ) and 611.14 nm ( $f = 1.3827$ ), respectively. Therefore, the change of the local electric field should result in a red-shifted absorption, following the reduced oscillator strengths.

### 3.4. Chemical Reactivity Parameters and Reorganization Energy

The Ionization Potential (IP) and the Electron Affinity (EA) were studied to explore the ability of organic solar cells to transport the holes and electrons [34]. Calculated values of IP and EA were listed in Table 1, which show that the XY1 has a smaller value of IP than that of D35; EA for D35 and XY1 are 3.042 and 3.068 eV, respectively, and estimation of EA and IP shows that there is improvement of charge transport for the XY1 structure in comparison with D35 structure. The chemical hardness ( $h$ ), electrophilicity ( $\omega$ ), and electroaccepting power ( $\omega^+$ ) are important parameters that have influence on the efficiency of photoelectric conversion (see Table 1). It is obvious that the  $h$  of D35 and XY1 are 0.804 and 0.774 eV, respectively. The  $\omega^+$  of D35 and XY1 are 7.380 eV and 7.715 eV, respectively. The D–A– $\pi$ –A model XY1 possesses lower  $h$  and higher  $\omega^+$  compared with D35, meaning a lower resistance to ICT and higher ability to receive charge. The  $\omega$  reflects the stability of the dye system, and the calculated  $\omega$  of D35 and XY1 are 9.203 and 9.539 eV, respectively, and that exhibits the same trend as the value of  $\omega^+$ .

**Table 1.** Chemical reactivity (in eV) of D35 and XY1 in acetonitrile solution; IP (Ionization Potential); EA (the Electron Affinity).

Dye	IP	EA	$h$	$\omega$	$\omega^-$	$\omega^+$
D35	4.649	3.042	0.804	9.203	11.226	7.380
XY1	4.615	3.068	0.774	9.539	11.557	7.715

### 3.5. Intramolecular and Intermolecular Charge Transfer (CT)

Photoinduced CT and separation are important processes for generating currents in the external circuit. The possible CT channels include the CT process between the dye and semiconductor, and for cosensitization systems international CT should be considered due to the electron transfer occurrence caused by the energy level discrepancy. 3D cube representation of CDD indicated that the first excited state of D35–TiO<sub>2</sub> is an ICT state, where the red electron was moved to the acceptor and surface of semiconductor, and the hole resided in the donor unit. Dynamic electron injection time can be estimated by the Newns–Anderson model [31,32], which was defined as:

$$\tau_{inj}(fs) = \frac{658}{\Delta(MeV)} \quad (1)$$

$$\Delta = \sum_{p_i} |\varepsilon_i - E_{LUMO}(ads)| \quad (2)$$

where  $\Delta$  and  $p_i$  stand for the energetic broadening and adsorbate portion of every molecular orbital, respectively;  $\varepsilon_i$  is orbital energy. When excited electrons were injected into the titanium dioxide, electron injection driving forces for D35 and XY1 are  $-1.71$  eV and  $-1.54$  eV (see Table S4); at the same time, the fast electron injection (fs) was calculated to be 9.51 fs (D35) and 9.12 fs (XY1), and the results indicated that fast electron injection is more likely to occur in the D35 system. It is hoped that the fast electron injection process is better than an intermolecular CT process during the intramolecular and intermolecular CT (D35 and XY1).

It is worthwhile to note that the orbital energy difference should result in the international CT, which can be estimated with CDD and Marcus theory [30,33]. From Figure 4, CDD revealed that all the electrons are localized on XY1 dye, and all the holes are situated on D35; the charge distribution on

electronic transition corresponding to the S<sub>5</sub> excited state that ICT state, where electrons transfer from D35 to unit XY1. The CT and recombination were calculated with the Marcus theory [30].

$$k = \sqrt{\frac{4\pi^3}{h^2\lambda k_B T}} |V_{DA}|^2 \exp\left(-\frac{(\Delta G_{CT} + \lambda)^2}{4\lambda k_B T}\right) \quad (3)$$

where  $K_B$  is the Boltzmann constant,  $h$  is Planck's constant,  $T$  is the temperature ( $T = 300$  K),  $\lambda$  is the reorganization energy; and electronic coupling  $V_{DA}$  for CT is calculated with Generalized Mulliken–Hush (GMH) [35], which is calculated to be  $135.5 \text{ cm}^{-1}$ ;  $\Delta G$  is the free energy change for CT process;  $\Delta G_{CT} = -\Delta G_{CR} - \Delta E_{0-0}$ , where the  $E_{0-0}$  lowest excitation energy of donor (see Table S2), and  $\Delta G_{CT} = -0.54$  eV. Calculated CT rate is  $4.895 \times 10^{12} \text{ s}^{-1}$ , which is smaller than the electron injection rate in the framework of fs. For the cosensitization system, comparison between the electron injection from molecule to TiO<sub>2</sub> and intermolecular CT (D35 and XY1) demonstrated that fast electron injection could decrease the loss of intermolecular CT.

In terms of the lifetime ( $t$ ), a longer lifetime is hoped for keeping a stable state in the cationic state. According to the relationship:  $t = 1.499/(f E^2)$ , calculated lifetime ( $t$ ) is listed in Table S4, which shows this order of D35 (2.27 ns) > XY1 (1.92 ns). From the above results, it found that  $t$  for D35 is longer than that of XY1, meaning that improvement of CT will enhance the  $J_{sc}$ . (short-circuit photocurrent) Furthermore, there is close excitation energy and smaller oscillator for cosensitization D35/XY1, and the lifetime for cosensitization system is longer than that of XY1.

### 3.6. Factors Influencing $J_{SC}$ and $V_{oc}$

For the short-circuit photocurrent ( $J_{SC}$ ) parameter, it is defined as [36]:

$$J_{SC} = \int_{\lambda} LHE(\lambda) \phi_{inject} \eta_{collect} d\lambda \quad (4)$$

where  $LHE(\lambda)$  is the light harvesting efficiency at a given wavelength, and  $\phi_{inject}$  is the electron injection efficiency.  $\eta_{collect}$  denotes the charge collection efficiency relative to photoanode properties, and thus it can be viewed as a constant.  $LHE(\lambda)$  is expressed as:

$$LHE = 1 - 10^{-f} \quad (5)$$

where  $f$  represents the oscillator strength of dye molecules corresponding to wavelength  $\lambda_{max}$ . From Table S2, the value of oscillator is in this order of XY1 > XY1 and D35 > D35, resulting in the LEH trend of XY1 > XY1 and D35 > D35. Furthermore, driving force can be estimated from the process of electron injection, and calculated value of driving force is in this order of D35 > XY1 and D35 > XY1, which means that electron injection takes place easily for the cosensitization compared with XY1.

The improved LEH and electron transfer should be the reason for improving the  $J_{sc}$  in the cosensitization system. Furthermore,  $V_{OC}$  can be closed to the conduction band edge of the semiconductor substrate ( $E_{CB}$ ), and  $\Delta E_{CB}$  is the shift of  $E_{CB}$  under adsorption [15,17,37]

$$\Delta E_{CB} = -\frac{q\mu_{normal}\gamma}{\epsilon_0\epsilon} \quad (6)$$

In this expression, dipole moment of  $\mu_{normal}$  is perpendicular to the surface of a semiconductor, and  $\gamma$  denotes the surface concentration of dyes.  $\epsilon_0$  and  $\epsilon_0$  represent the vacuum permittivity and the dielectric permittivity, respectively. It is obvious that  $\mu_{normal}$  is the key factor in determining  $V_{OC}$ , and the calculated results is in this order of XY/D35 (27.3679D) > XY1 (-17.1053D) > D35 (13.9281D), meaning that the larger  $\mu_{normal}$  results in the larger  $V_{OC}$  in cosensitization system.

#### 4. Conclusions

CT and photoelectric characteristics of a cosensitization solar cell have been investigated theoretically with the aid of DFT in combination with the visualized methods. Intramolecular and intermolecular CT processes can be estimated from the Newns–Anderson model and Marcus theory. It was found that: energy levels of XY1, D35, and XY1 and D35 have good matching with a semiconductor band, which is in favor of electron injection; absorption spectra of XY1 and D35 have a wide absorption range in the visible region with two prominent peaks, enhancing photoabsorption efficiency; 3D cube representation shows that the S1 state for the isolated dye (XY1 or D35) is intramolecular CT, where red electron was moved from dyes into the semiconductor on the scale of fs. The injection time and driving force demonstrated that D35 takes place in electron injection easily; comparing with intramolecular CT, intermolecular CT demonstrated that the fast electron injection can decrease the loss of intermolecular CT. The improved absorption ability, electron transfer, and dipole moment for the cosensitization system should improve photoelectric efficiency.

**Supplementary Materials:** The following are available online at <http://www.mdpi.com/2076-3417/8/7/1122/s1>.

**Author Contributions:** Y.L., P.S. and F.M. conceived and designed this work. Q.L. and X.L. developed the CT model and simulation program. L.M. and N.G. analyzed the data. Q.L., X.L. and L.M. wrote the paper.

**Funding:** This work was supported by the China Postdoctoral Science Foundation (2016 M590270), the Heilongjiang Postdoctoral Grant (LBH-Z15002), and the National Natural Science Foundation of China (Grant Nos. 11404055, 61675165 and 11304135). Nan Gao and Lu Mi thank the college students' innovation project of NEFU (201709000001) and college student research training Program of NEFU (KY2017001) for the support.

**Conflicts of Interest:** The authors declare no conflict of interest.

#### References

1. Regan, B.O.; Grätzel, M. A low-cost, high-efficiency solar cell based on dye-sensitized colloidal TiO<sub>2</sub> films. *Nature* **1991**, *353*, 737–740. [[CrossRef](#)]
2. Cao, Y.M.; Saygili, Y.; Ummadisingu, A.; Teuscher, J.; Luo, J.S.; Pellet, N.; Giordano, F.; Zakeeruddin, S.M.; Moser, J.E.; Freitag, M.; et al. 11% efficiency solid-state dye-sensitized solar cells with copper(II/I) hole transport materials. *Nat. Commun.* **2017**, *8*, 15390. [[CrossRef](#)] [[PubMed](#)]
3. Shen, Z.; Xu, B.; Liu, P.; Hu, Y.; Yu, Y.; Ding, H.; Kloo, L.; Hua, J.; Sun, L.; Tian, H. High performance solid-state dye-sensitized solar cells based on organic blue-colored dyes. *J. Mater. Chem. A* **2017**, *5*, 1242–1247. [[CrossRef](#)]
4. Gong, J.W.; Sumathy, K.; Qiao, Q.; Zhou, Z.P. Review on dye-sensitized solar cells (DSSCs): Advanced techniques and research trends. *Renew. Sustain. Energy Rev.* **2017**, *68*, 234–246. [[CrossRef](#)]
5. Li, Y.Z.; Li, H.; Zhao, X.; Chen, M.D. Electronic structure and optical properties of dianionic and dicationic  $\pi$ -Dimers. *J. Phys. Chem. A* **2010**, *114*, 6972–6977. [[CrossRef](#)] [[PubMed](#)]
6. Xie, Y.S.; Tang, Y.Y.; Wu, W.J.; Wang, Y.Q.; Liu, J.C.; Li, X.; Tian, H.; Zhu, W.H. Porphyrin Cosensitization for a Photovoltaic Efficiency of 11.5%: A Record for Non-Ruthenium Solar Cells Based on Iodine Electrolyte. *J. Am. Chem. Soc.* **2015**, *137*, 14055–14058. [[CrossRef](#)] [[PubMed](#)]
7. Luo, J.S.; Wan, Z.Q.; Jia, C.Y.; Wang, Y.; Wu, X.C.; Yao, X.J. Co-sensitization of Dithiafulvenyl–Phenothiazine Based Organic Dyes with N719 for Efficient Dye-Sensitized Solar Cells. *Electrochim. Acta* **2016**, *211*, 364–374. [[CrossRef](#)]
8. Liu, B.; Chai, Q.; Zhang, W.; Wu, W.; Tian, H.; Zhu, W. Cosensitization process effect of DA– $\pi$ –A featured dyes on photovoltaic Performances. *Green Energy Environ.* **2016**, *1*, 84–90. [[CrossRef](#)]
9. Kakiage, K.; Aoyama, Y.; Yano, T.; Oya, K.; Kyomen, T.; Hanaya, M. Fabrication of a high-performance dye-sensitized solar cell with 12.8% conversion efficiency using organic silyl-anchor dyes. *Chem. Commun.* **2015**, *51*, 6315–6317. [[CrossRef](#)] [[PubMed](#)]
10. Hao, Y.; Saygili, Y.; Cong, J.; Eriksson, A.; Yang, W.; Zhang, J.; Polanski, E.; Nonomura, K.; Zakeeruddin, S.M.; Grätzel, M.; et al. Novel Blue Organic Dye for Dye-Sensitized Solar Cells Achieving High Efficiency in Cobalt-Based Electrolytes and by Co-Sensitization. *ACS Appl. Mater. Interfaces* **2016**, *8*, 32797–32804. [[CrossRef](#)] [[PubMed](#)]

11. Wang, Y.Q.; Chen, B.; Wu, W.J.; Li, X.; Zhu, W.H.; Tian, H.; Xie, Y.S. Efficient Solar Cells Sensitized by Porphyrins with an Extended Conjugation Framework and a Carbazole Donor: From Molecular Design to Cosensitization. *Angew. Chem. Int. Ed.* **2014**, *53*, 10779–10783. [[CrossRef](#)] [[PubMed](#)]
12. Freitag, M.; Teuscher, J.; Saygili, Y.; Zhang, X.; Giordano, F.; Liska, P.; Hua, J.; Zakeeruddin, S.M.; Moser, J.-E.; Grätzel, M.; et al. Dye-sensitized solar cells for efficient power generation under ambient lighting. *Nat. Photonics* **2017**, *11*, 372–378. [[CrossRef](#)]
13. He, L.J.; Wei, W.; Chen, J.; Jia, R.; Wang, J.; Zhang, H.X. The effect of D-[De- $\pi$ -A] $n$  ( $n = 1, 2, 3$ ) type dyes on the overall performance of DSSCs: A theoretical investigation. *J. Mater. Chem. C* **2017**, *5*, 7510–7520. [[CrossRef](#)]
14. Xu, B.B.; Li, Y.Z.; Song, P.; Ma, F.C.; Sun, M.T. Photoactive layer based on T-shaped benzimidazole dyes used for solar cell: From photoelectric properties to molecular design. *Sci. Rep.* **2017**, *7*, 45688. [[CrossRef](#)] [[PubMed](#)]
15. Yang, L.N.; Zhou, H.Y.; Sun, P.P.; Chen, S.L.; Li, Z.S. A Promising Candidate with D-A-A-A Architecture as an Efficient Sensitizer for Dye-Sensitized Solar Cells. *ChemPhysChem* **2015**, *16*, 601–606. [[CrossRef](#)] [[PubMed](#)]
16. Liu, Q.; Ren, P.H.; Wang, X.F.; Li, Y.Z.; Yang, Y.H. Experimental and Theoretical Investigation of Photoelectrical Properties of Tetrabromophenol blue and Bromoxylene blue based solar cell. *J. Nanomater.* **2018**, 9720595, in press.
17. Li, Y.Z.; Sun, C.F.; Song, P.; Ma, F.C.; Yang, Y.H. Tuning the electron transport and accepting ability of dyes via introducing different  $\pi$ -conjugated bridges and acceptors for DSSCs. *ChemPhysChem* **2017**, *18*, 366–383. [[CrossRef](#)] [[PubMed](#)]
18. Bahers, T.L.; Brémond, E.; Ciofini, I.; Adamo, C. The nature of vertical excited states of dyes containing metals for DSSC applications: Insights from TD-DFT and density based indexes. *Phys. Chem. Chem. Phys.* **2014**, *16*, 14435–14444. [[CrossRef](#)] [[PubMed](#)]
19. Ali, B.A.; Allam, N.K. Propping the optical and electronic properties of potential photo-sensitizers with different  $\pi$ -spacers: TD-DFT insights. *Spectrochim. Acta A* **2018**, *188*, 237–243. [[CrossRef](#)] [[PubMed](#)]
20. Sharmoukh, W.; Hassan, W.M.I.; Gros, P.C.; Allam, N.K. Design and synthesis of new Ru-complexes as potential photo-sensitizers: Experimental and TD-DFT insights. *RSC Adv.* **2016**, *6*, 69647–69657. [[CrossRef](#)]
21. Frisch, M.J.; Trucks, G.W.; Schlegel, H.B.; Scuseria, G.E.; Robb, M.A.; Cheeseman, J.R.; Scalmani, G.; Barone, V.; Mennucci, B.; Petersson, G.A.; et al. *Gaussian 09*; Revision A.02; Gaussian, Inc.: Wallingford, CT, USA, 2009.
22. Parr, R.G. Density functional theory. *Ann. Rev. Phys. Chem.* **1983**, *34*, 631–656. [[CrossRef](#)]
23. Becke, A.D. Density-functional exchange-energy approximation with correct asymptotic behavior. *Phys. Rev. A* **1988**, *38*, 3098–3100. [[CrossRef](#)]
24. Becke, A.D. Density-functional thermochemistry. III. The role of exact exchange. *J. Chem. Phys.* **1993**, *98*, 5648–5652. [[CrossRef](#)]
25. Lee, C.; Yang, W.; Parr, R.G. Development of the Colle-Salvetti correlation-energy formula into a functional of the electron density. *Phys. Rev. B Condens. Matter* **1988**, *37*, 785–789. [[CrossRef](#)] [[PubMed](#)]
26. Stratmann, R.E.; Scuseria, G.E.; Frisch, M.J. An efficient implementation of time-dependent density-functional theory for the calculation of excitation energies of large molecules. *J. Chem. Phys.* **1998**, *109*, 8218–8224. [[CrossRef](#)]
27. Yanai, T.; Tew, D.P.; Handy, N.C. A new hybrid exchange–correlation functional using the Coulomb-attenuating method (CAM-B3LYP). *Chem. Phys. Lett.* **2004**, *393*, 51–57. [[CrossRef](#)]
28. Barone, V.; Cossi, M. Quantum Calculation of Molecular Energies and Energy Gradients in Solution by a Conductor Solvent Model. *J. Phys. Chem. A* **1998**, *102*, 1995–2001. [[CrossRef](#)]
29. Yao, B.-Q.; Sun, J.-S.; Tian, Z.-F.; Ren, X.-M.; Gu, D.-W.; Shen, L.-J.; Jiang, X. Ion-pair charge transfer complexes with intense near IR absorption: Syntheses, crystal structures, electronic spectra and DFT calculations. *Polyhedron* **2008**, *27*, 2833–2844. [[CrossRef](#)]
30. Marcus, R.A. Electron transfer reactions in chemistry. Theory and experiment. *Rev. Mod. Phys.* **1993**, *65*, 599–610. [[CrossRef](#)]
31. Muscat, J.P.; Newns, D.M. Chemisorption on metals. *Prog. Surf. Sci.* **1978**, *9*, 1–43. [[CrossRef](#)]
32. Ding, W.L.; Peng, X.L.; Sun, Z.Z.; Li, Z.S. Novel bifunctional aromatic linker utilized in CdSe quantum dots-sensitized solar cells: Boosting the open-circuit voltage and electron injection. *J. Mater. Chem. A* **2017**, *5*, 14319–14330. [[CrossRef](#)]

33. Zong, H.; Wang, J.C.; Mu, X.J.; Xu, X.F.; Li, J.; Wang, X.Y.; Long, F.X.; Wang, J.X.; Sun, M.T. Physical mechanism of photoinduced intermolecular charge transfer enhanced by fluorescence resonance energy transfer. *Phys. Chem. Chem. Phys.* **2018**, *20*, 13558–13565. [[CrossRef](#)] [[PubMed](#)]
34. Deng, D.; Zhang, Y.J.; Zhang, J.Q.; Wang, Z.Y.; Zhu, L.Y.; Fang, J.F.; Xia, B.Z.; Wang, Z.; Lu, K.; Ma, W.; et al. Fluorination-enabled optimal morphology leads to over 11% efficiency for inverted small-molecule organic solar cells. *Nat. Commun.* **2016**, *7*, 13740. [[CrossRef](#)] [[PubMed](#)]
35. Cave, R.J.; Newton, M.D. Generalization of the Mulliken–Hush treatment for the calculation of electron transfer matrix elements. *Chem. Phys. Lett.* **1996**, *249*, 15–19. [[CrossRef](#)]
36. Obotowo, I.N.; Obot, I.B.; Ekpe, U.J. Organic sensitizers for dye-sensitized solar cell (DSSC): Properties from computation, progress and future perspectives. *J. Mol. Struct.* **2016**, *1122*, 80–87. [[CrossRef](#)]
37. Rühle, S.; Greenshtein, M.; Chen, S.G.; Merson, A.; Pizem, H.; Sukenik, C.S.; Cahen, D.; Zaban, A. Molecular Adjustment of the Electronic Properties of Nanoporous Electrodes in Dye-Sensitized Solar Cells. *J. Phys. Chem. B* **2005**, *109*, 18907–18913. [[CrossRef](#)] [[PubMed](#)]



© 2018 by the authors. Licensee MDPI, Basel, Switzerland. This article is an open access article distributed under the terms and conditions of the Creative Commons Attribution (CC BY) license (<http://creativecommons.org/licenses/by/4.0/>).